Flow through Self-Affine Fractures

H. J. Seybold,[1] H. A. Carmona,[2] F. A. Leandro Filho,[2] A. D. Araújo,[2] F. Nepomuceno Filho,[2] and J. S. Andrade Jr.[2,*]

[1] *Physics of Environmental Systems, D-USYS, ETH, Zurich, 8093 Zurich, Switzerland*
[2] *Departamento de Física, Universidade Federal do Ceará, Campus do Pici, 60451-970 Fortaleza, Ceará, Brazil*

Surface roughness has a considerable influence on the flow resistance of fluids passing through fracture joints. Using the Hurst exponent H to characterize the roughness of a self-affine surface, we investigate the impact of inertia on the flow's resistance as a function of roughness and Reynolds number. We find that the hydraulic resistance $G \equiv -\Delta P w^2/\mu U L$ follows a universal behavior when the characteristic length scale of the system is defined by the tortuosity of the surface times the opening of the fracture. Moreover, we show that the nonlinear corrections to Darcy's law are proportional to the Hurst exponent at the transition from Stokes to inertial flow. This result implies that the second and third order corrections to Darcy's law depend depend on the permeability even for very rough surfaces ($H \sim 0.3$). The effective permeability of the fracture decays exponentially with H^{-1}. Our results also reveal the presence of quasi-one-dimensional channeling of the flow, even when there is no shear displacement between the upper and lower surfaces constituting the self-affine fracture joints.

I. INTRODUCTION

Understanding the detailed behavior of a fluid flowing through a fractured rock, in particular in what way the morphology of the fracture's surfaces influences the flow resistance is of great importance in many practical applications [1–5].

Fractures have crucial role in driving fluids through naturally fractured carbonate reservoirs [6, 7], and hydraulic fracturing [8, 9] is a procedure frequently used for oil recovery. Since at the reservoir scale fractures are mostly composed of networks of interconnected cracks with very different sizes, it is relevant to understand how the behavior of the flow in a single fracture scales with its size, as well as how it is affected by the surface morphology [7]. The local flow structures are a direct result of the fracture's morphology and many studies have been dedicated to understand their upscale in order to derive macroscopic relations [10–13].

It has become increasingly clear that the morphology of brittle fractures follows *self-affine* scaling laws [14]. More precisely, it means that by re-scaling an in-plane vector $\mathbf{r}$ by $\lambda\mathbf{r}$, the out-of-plane coordinate z needs to be re-scaled by $\lambda^H z$ for the surface to remain statistically invariant, where the scaling exponent H is called the Hurst exponent. It was first suggested that rock fractures have a unique exponent $H = 0.8$ [15–21]. However, recent evidence indicates that other values of H also occur in natural systems (ranging from 0.45 to 0.85) depending on the material and how the fracture has been produced [22–25]. As a result, more than one universality class exists for fractured rocks and therefore it is important to understand how the flow properties are affected by variations in the Hurst exponent.

A single-phase flow in a fractured rock is usually characterized in terms of Darcy's law [3, 26, 27], which defines a linear relation between the mean flow velocity U and the pressure drop ΔP across the system, namely $U = -k\Delta P/\mu L$. Here μ is the fluid's viscosity, L is the length of the fracture in the flow direction, and the proportionally constant k is the permeability. Essentially Darcy's law is a good approximation at low Reynolds numbers, $\mathrm{Re} = \rho U w/\mu \ll 1$, where w is usually taken as the aperture of the fracture and ρ is the density of the fluid. However, in order to understand the interplay between the surface's roughness and the flow inside the fracture, it is necessary to examine *local* aspects of the surface roughness and relate them to the relevant mechanisms of momentum transfer through viscous and inertial forces.

The influence of surface roughness on the flow properties inside a fracture has been first studied theoretically by Roux *et al.* [10]. They predicted that the permeability of a self-affine fracture should scale with the length of the system as $k \sim L^{2H}$. This result is based on the assumption that the fracture behaves like a system of parallel plates with an effective aperture w, given that self-affinity implies that $w \sim L^H$, and $k \sim w^2$ follows the solution of the Stokes equation.

Since then, several theoretical and experimental studies, all focused on how the permeability scales with the fracture opening and length in the viscous flow regime, treating it as an equivalent system of parallel plates. Using perturbation theory, Drazer and Koplik [28] calculated that the permeability should scale as $k_0 - k \sim L^H$ for two-dimensional flows, where k_0 is the permeability of the unperturbed system. Later they extended their study to three-dimensional flows and confirmed their results in terms of the effective medium analysis with numerical simulations at low Reynolds numbers. Talon *et al.* [11] conjectured that the permeability is controlled by the minimum aperture of the fracture, and found that, for two-dimensional flows, k scales with this minimum aperture with an exponent $3 - 1/H$, using order statistics for uncorrelated power-law distributions for the aper-

* soares@fisica.ufc.br

ture. For three-dimensional flows, however, Talon *et al.* have shown numerically that $k \sim b_c^{2.25}$ for $H = 0.8$ and $k \sim b_c^{2.16}$ for $H = 0.3$, where b_c is an equivalent aperture.

The role of non-linear effects in fluid flow through two-dimensional self-affine fractures have been addressed by Sketne *et al.* [29], who considered fractures with constant aperture and $H = 0.8$. Their numerical simulations show that in the range of intermediate Reynolds number ($\mathrm{Re} \approx 1$), the flow can be described by a weak inertia equation [30, 31], whereas for moderate Reynolds numbers ($25 \leq \mathrm{Re} \leq 52$) the inertial effects can be described by the Forchheimer equation [32]. More recent numerical results [33] extend these results for different Hurst exponents ($0.65 \leq H \leq 1$).

It is evident that non-linear effects have very different impact on two- and three-dimensional flow systems. Here we address the question of how the permeability and the nonlinear corrections to Darcy's law depend on the surface roughness. To do so we systematically examine the behavior of the fluids hydraulic resistance as a function of the Reynolds number (Re) ranging from 10^{-2} to 500, for different values of the Hurst exponent, varying from 0.3 to 0.9.

The balance of this paper is organized as follows. Sec. II describes the methods we have used to generate the geometry, and the setup of the computer simulations. In Sec. III we present and discuss our simulation results and Section IV is devoted to the conclusions.

II. METHODS

Each of the three-dimensional numerical fractures used in out analysis consists of the volume between two identical self-affine surfaces, representing the fracture walls. The surfaces have been displaced in the direction perpendicular to the mean surface plane (the $x - y$ plane). Specifically, no additional shear displacement is added to the surfaces in this plane, so that the fracture aperture w is constant throughout the numerical domain, as depicted in Fig. 1.

The wall surfaces are generated by applying a two-dimensional generalization of the fractional Brownian Motion [34–37] satisfying the following scaling relation:

$$\left\langle \left[z\left(\mathbf{r}_2\right) - z\left(\mathbf{r}_1\right) \right]^2 \right\rangle \propto \left| \mathbf{r}_2 - \mathbf{r}_1 \right|^{2H} . \tag{1}$$

Here $z(\mathbf{r})$ defines the elevation of the wall surface and $\mathbf{r}$ is a vector in the $x - y$ plane. The Hurst exponent H characterizes the spatial correlations of the surface. Surfaces with $H < 0.5$ are spatially anti-correlated, while for $H > 0.5$ long-range spatial correlations are present. For the case $H = 0.5$ we obtain ordinary Brownian surfaces formed by successive uncorrelated increments [37]. In order to create a discrete fractional Brownian surface with a given exponent H numerically,we use a Fourier filtering method [37, 38]. This method imposes a scaling property on the spectral density S_z,

$$S_z(k) \propto \frac{1}{k^{\xi}}, \tag{2}$$

where the parameter ξ is related to the Hurst exponent via $\xi = 2 + 2H$ for two-dimensional surfaces [39]. Equation 2 is used to define the amplitudes of the coefficients of the discrete Fourier transform of the wall surfaces, which are subsequently transformed the back to real space using a fast Fourier transform.

The length of the fracture in the x and y directions is set to $L = 512$ in dimensionless units for all wall surfaces in this investigation. In order to obtain fractures with a comparable variability in z direction the amplitude of the surfaces are set in such a way that $\sigma_z = \frac{1}{L} \sum_{i,j} \left| z_{i,j} - \langle z \rangle \right|^2 \approx 5$ is fixed for all surfaces. Here $z_{i,j}$ is the height of the surface at the discrete location (x_i, y_j). Finally the fracture opening is also identical for all numerical samples, $w = 40$.

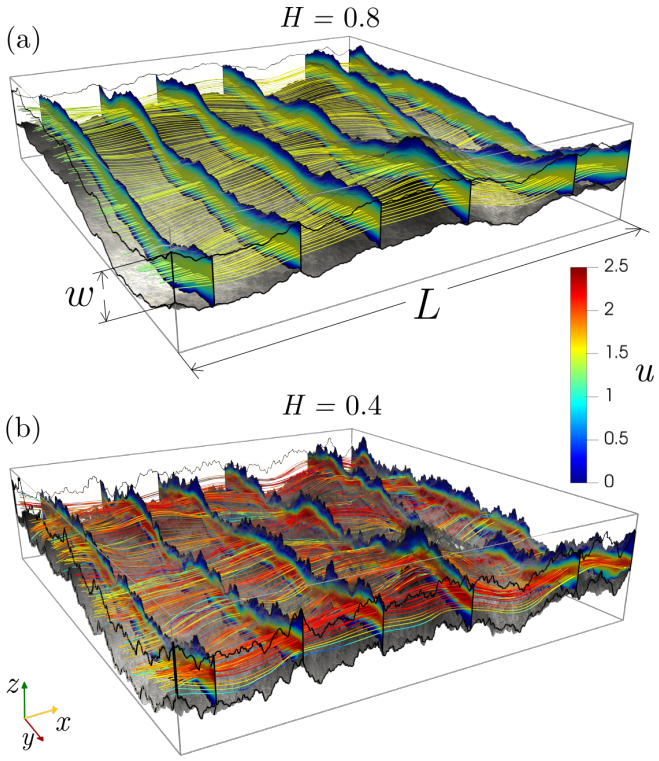

FIG. 1. Fluid flow through a typical fracture joint calculated for Re = 100 and Hurst exponents (a) $H = 0.8$ and (b) $H = 0.4$. The fluid flows from left to right. The contour plots correspond to the velocity magnitude at different cross sections. Streamlines are also shown, colored according to the local velocity magnitude.

The three-dimensional flow through the self-affine fractures is described by the incompressible Navier-Stokes equations under isothermal steady-state conditions. Consequently, the momentum and mass conservation equations are read as

$$\rho\ \mathbf{u} \cdot \nabla \mathbf{u} = -\nabla p + \mu\ \nabla^2 \mathbf{u}\ , \tag{3}$$

$$\nabla \cdot \mathbf{u} = 0\ , \tag{4}$$

where $\mathbf{u}$, p and ρ are the velocity, pressure, and the fluid's density, respectively. As boundary condition, we apply non-slip conditions at the top and bottom walls. Fluid is injected in the x direction at $x = 0$ using a uniform velocity profile with amplitude U at the inlet, and a constant pressure defines the outlet boundary, at $x = L$. Laterally symmetrical boundary conditions were applied to minimize finite-size effects. In order to solve Eqs. (3) and (4) numerically, we first discretize the volume between the top and bottom surface of the crack using a tree-dimensional unstructured hexahedral mesh generated by the OpenFOAM's meshing tool *snappyHexMesh* [40]. Close to the surface, the hexahedral cells were refined three times in order to capture small variations of the fracture surface over several orders of magnitude.

For different values of the Hurst exponent in the range $0.3 \leq H \leq 0.9$, we generated five realizations of the computational domain to compute ensemble averages. This results in a total of $7 \times 5 = 35$ computational domains. We then, for each realization, systematically vary the Reynolds number from Re = 0.01 up to Re = 500 by adjusting the inlet velocity U.

III. RESULTS AND DISCUSSION

The Forchheimer equation [32, 41] has been widely used to describe inertial corrections to Darcy's law for the bulk flow through disordered pore structures [3, 27, 42]. Up to cubic order these corrections can be written as,

$$-\frac{\Delta P}{L} = \alpha\mu U + \beta\rho U^2 + \frac{\gamma\rho^2 U^3}{\mu}\ , \tag{5}$$

where α corresponds to the reciprocal of the permeability of the channel, and β and γ are the coefficients of the second- and third-order corrections, respectively. Empirical evidence indicates that the addition of third-order corrections in the velocity to the Forchheimer equation allows for an excellent agreement with experimental data for the full range of the laminar regime [26, 43–45]. Here we adopt this approach to characterize the effect of the convective influence on the flow through the self-affine channel.

Rewriting Eq.(5) in terms of Re, we obtain,

$$G = \alpha w^2 + \beta w \mathrm{Re} + \gamma \mathrm{Re}^2, \tag{6}$$

where $G \equiv -\Delta P w^2/\mu U L$ is a dimensionless measure of the *hydraulic resistance*. Figure 2 displays the results from $t \times 5 \times 20 = 700$ numerical simulations, where G is plotted as a function of Reynolds number. For each value of the parameters Re and H, the value of G is obtained as the average over a total of five realizations. Using the ensemble averages of G, we then fit Eq. (6) to the data in order to determine the coefficients α, β and γ.

For small Reynolds numbers, G is dominated by the first term in Eq. 6, namely αw^2. This quantity decreases monotonically with the Hurst exponent H as shown in the inset of Fig. 3, approaching the limiting value $\alpha = 12/w^2$, for a fracture constituted of two parallel planes with constant aperture w, as H tends to one.

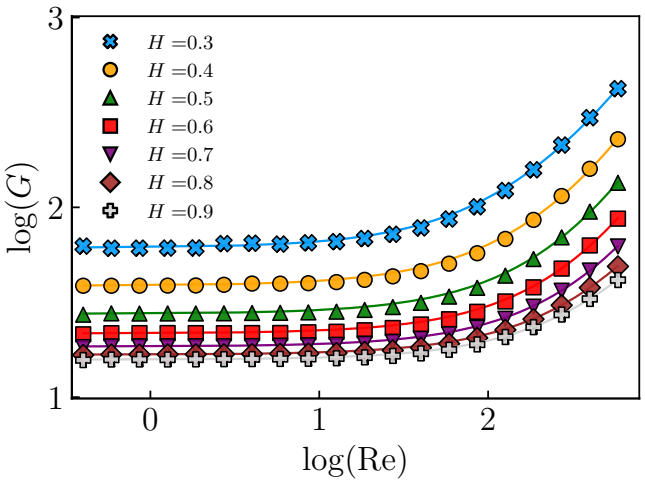

FIG. 2. Dependence of the hydraulic resistance G on the Reynolds number Re for different values of the Hurst exponent H. In all cases, the plateau corresponding to Darcy's law (constant G) is followed by a non-linear regime that reflects the effect of convection on the flow. The error bars are smaller than the symbols and the solid lines are the best fit to the data using Eq. (6).

In order to understand the particular form of this dependence we consider the fracture as composed of a sequence of parallel plates with varying angles with respect to the x-y plane. For this very simplified model the quantity the inverse of the permeability can be approximated by the expression

$$\alpha w^2 \propto \tau \tag{7}$$

where $\tau \equiv L_p/L$, with L_p being the perimeter of the fracture in the direction of the flow. In this way, τ represents the tortuosity of the fracture. For a self-affine fracture surface one finds

$$\tau = \sqrt{1 + \frac{\sigma_z^2}{\delta x^2}\left(\frac{\delta x}{L}\right)^{2H}} \tag{8}$$

where δx is the resolution used to compute the perimeter L_p.

Figure 3 shows the αw^2 follows very closely Eq. (7) for small values of H. The solid line represents a fit to the data combining Eqs. (7) and (8) with $\sigma = 5$ and $\delta x = 2$. The fit corresponds to $\alpha w^2 = a + b\tau$ with $a = -42.4 \pm 0.7$ and $b = 58.9 \pm 0.6$ with a Person's $R^2 = 0.97$. For larger values of the Hurst exponent ($H > 0.7$) the tortuosity of the fluid flow is smaller than the tortuosity of the surface due to dynamical effects even for very low Reynolds numbers, and the simplified model described above is expected to overestimate αw^2.

In agreement with experiments [46], we observe that the transition from a linear (constant G) to a non-linear

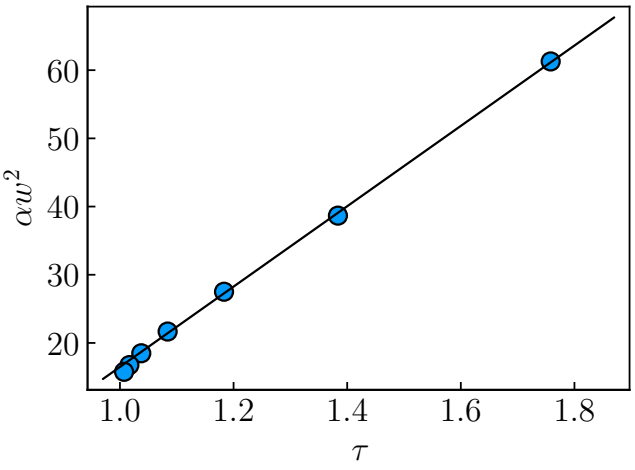

FIG. 3. Variation of αw^2 with the tortuosity τ. The error bars are smaller than the symbols sizes. The inset shows the dependence of αw^2 with the Hurst exponent H. The solid lines correspond to the least-squares fit using $\alpha w^2 = a + b\tau$, with $a = -42.4 \pm 0.7$ and $b = 58.9 \pm 0.6$, where τ was computed with $\sigma_z = 5$ and $\delta = 2$.

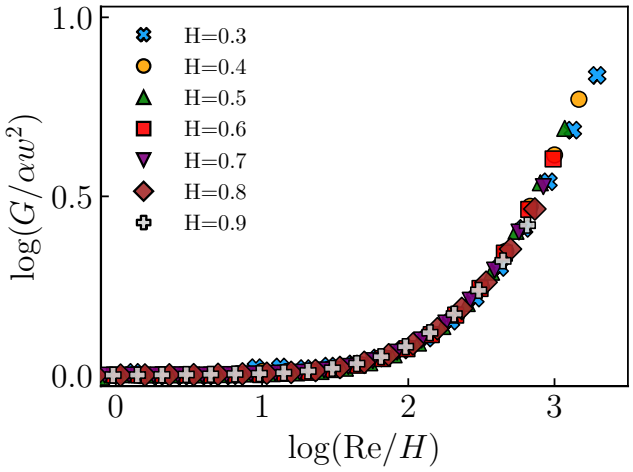

FIG. 4. Hydraulic resistance G as a function of Re/H. The excellent collapse of the simulation data onto a single curve is an indication that the onset of the nonlinear contributions to the hydraulic resistance increases approximately linearly with the Hurst exponent.

regime occurs at lower Re for increasing surface roughness. Although the absolute value of G significantly depends on the tortuosity, and decreases with H, the general increasing trend of the nonlinear corrections as a funcion of Re seems to be independent of the Hurst exponent.

In order to quantify the impact of the surface roughness on the departure from Darcy's law, we plot G as a function of Re/H. Following this procedure, all hydraulic conductivity curves collapse onto a single master curve, as shown in Fig. 4. This collapse is an indication that the onset of the non-linear contributions to the hydraulic resistance decreases in a linear fashion with the tortuosity parameter τ. As a matter of fact, the excellent quality of the collapse implies the scaling relations $\beta w \propto \alpha w^2/H$ and $\gamma \propto \alpha w^2/H^2$. As depicted in Fig. 5, the second-order term follows the proposed scaling relations rather well. For the third-order coefficient, however, we observe significant deviations from the proposed linear trend for $H < 0.4$ ($\alpha w^2/H^2 > 110$).

Next, we analyze the impact of the surface roughness on the velocity field directly. Figures 1a and b show typical realizations of fluid flows through fracture joints at $\mathrm{Re} = 100$ for Hurst exponents $H = 0.4$ and $H = 0.8$, respectively. The contour plots show the magnitude of the velocity field in different cross sections perpendicular to the main flow direction and streamlines of the velocity field are colored by the velocity magnitude. For the larger Hurst exponent, $H = 0.8$, the fluctuations in the local velocity field are visually smoother, with the maximum velocity near the center of the channel approximately equal to $3U/2$, as expected for parallel plates. For $H = 0.4$, however, the situation is rather different. Due to continuity, regions of higher velocities are clearly more confined at the center of the channel, since the zones of almost stagnated flow close to walls broadens. As a consequence, the maximum velocity magnitude approaches $5U/2$, effectively increasing the Reynolds number, as suggested by the collapse in Fig. 4. An enhancement in the velocity magnitude due to local disorder in the surface morphology can then persist and propagate further into the fracture joint forming preferential flow paths, where the fluid follows trajectories connecting "valleys" and around "mountains" of the rough surfaces. This effect is only possible in three-dimensional flows, since in two dimensions the flow is forced through local bottlenecks.

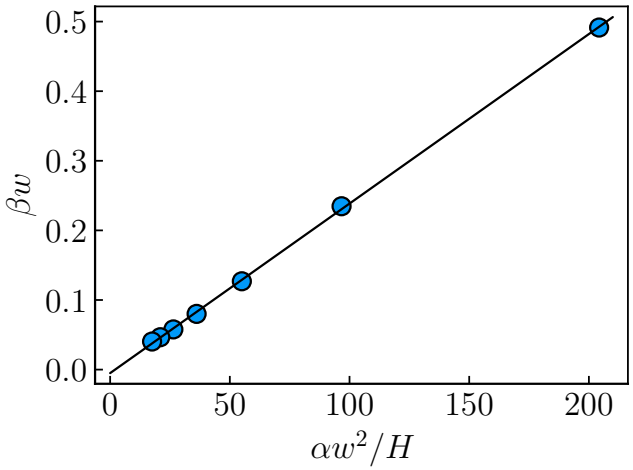

FIG. 5. (a) The parameter βw as a function of $\alpha w^2/H$. The solid line corresponds to the least-squares fit to the data using $\beta w = c_0 \left(\alpha w^2/H\right)$ with $c_0 = 0.0023 \pm 0.0001$. The resulting Pearson coefficients is $R^2 = 0.9997$. The inset shows the scaling of γ with $\alpha w^2/H^2$. The dashed line corresponds to $\gamma = c_1 \left(\alpha w^2/H^2\right) + c_2$ with $c_1 = (-1.01 \pm 0.05) \times 10^{-6}$ and $c_2 = (-1.03 \pm 0.1) \times 10^{-6}$. The simulation data deviates from the expected linearity for small $H < 0.4$ ($\alpha w^2/H^2 > 110$).

A similar channelization effect has been found in previous experiments [47] and computational simulations [48–

50]. This effect, however, was always associated to an additional shear displacement between the upper and lower surface, which generates a heterogeneous aperture distribution throughout those fractures. Our simulations, however, show that no lateral displacement is needed and that the channelization effect thus must a result of an effective aperture field which is significantly affected by surface topology.

The effect of channelization can be quantified by the participation ratio π, which describes the spatial localization of kinetic energy inside the flow [44]. The participation ratio is defined as

$$\pi = \frac{\langle e \rangle^2}{\langle e^2 \rangle}, \tag{9}$$

where $\langle e^n \rangle = (1/V) \iiint (\mathbf{u} \cdot \mathbf{u})^n \; d^3\mathbf{r}$ is the n^{th} moment of the kinetic energy and V is the volume of the system. If the kinetic energy is uniformly distributed across the sample, one obtains $\pi \to 1$, whereas if the flow field is strongly localized, $\pi \to 1/V$, approaching zero in the limit of a infinitely large system.

Figure 6 shows the variation of π as a function of H for $\mathrm{Re} = 100$, where the results are obtained by statistically averaging over five realizations. For $H \to 1$ the normalized Hurst exponent approaches a value of $\pi_0 = 0.7$ which is the expected value for a Poiseuille flow between two parallel plates. By decreasing H, the participation ratio decreases monotonically indicating a stronger preferential channeling effect. Also shown in Fig. 6 is the participation ratio computed only in the $w/2$-iso distance, defined by the vertical half distance between the lower and upper boundary of the crack. Compared to the bulk flow, the kinetic energy is mostly homogeneously distributed in this surface as the effect fo the wall roughness is minimal. In this case, π also increases with the Hurst exponent, reflecting the formation of flow channels in fractures generated with low values of H.

IV. CONCLUSIONS

In summary, we have presented an intensive numerical study of single-phase flow in self-affine fracture joints. We find that each of the coefficients α, β and γ, characterizing the cubic generalization of the Darcy's equation (5) increase exponentially with H^{-1}. Our results indicate that, in the range of Reynolds number we investigated, these coefficients are not all independent. Moreover, inertial effects on the overall flow can be understood in terms of a universal curve (independent of H) relating the fracture hydraulic conductance and Reynolds number. We also find that preferred flow paths arise in the flow field, indicating that, even in three-dimensional fracture joints with no shear displacement between top and bottom surfaces, the effective fracture aperture field is heterogeneous.

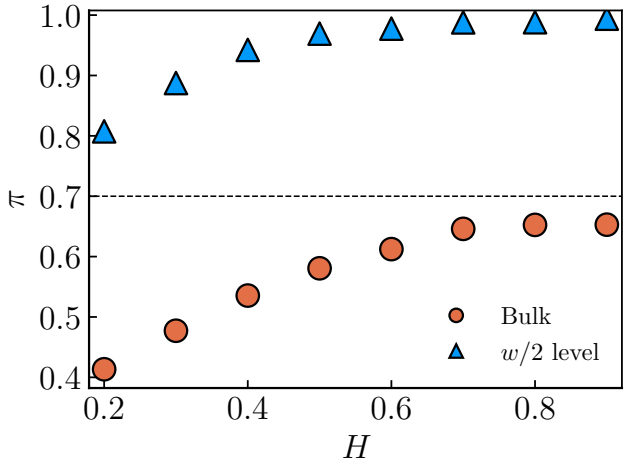

FIG. 6. Participation index π as a function of the Hurst exponent H. Red circles correspond to the bulk participation index and the blue squares denote the participation index in the $w/2$-level surface, obtained by translating the bottom surface of the channel by $w/2$ in the z-direction. The dashed horizontal line corresponds to $\pi = \pi_0$, the value of participation for the flow at low Re between two parallel plates.

ACKNOWLEDGMENTS

We thank the Brazilian agencies CNPq, CAPES and FUNCAP, also the National Institute of Science and Technology for Complex Systems and Petrobras for financial support.

[1] M. Sahimi, Rev. Mod. Phys. **65**, 1393 (1993).
[2] B. Berkowitz, Adv. Water Resour. **25**, 861 (2002).
[3] M. Sahimi, *Flow Transp. Porous Media Fract. Rock From Class. Methods to Mod. Approaches Second Ed.* (Wiley-VCH Verlag GmbH & Co. KGaA, Weinheim, Germany, 2011).
[4] S. G. Osborn, A. Vengosh, N. R. Warner, and R. B. Jackson, Proc. Natl. Acad. Sci. U.S.A. **108**, 8172 (2011).
[5] L. Williams, P. Macnaghten, R. Davies, and S. Curtis, Public Underst. Sci. **26**, 89 (2017).
[6] J. E. Warren and P. J. Root, SPE-426-PA (1963).
[7] R. Liu, B. Li, Y. Jiang, and N. Huang, Hydrol. J. **24**, 1623 (2016).
[8] M. K. Hubbert and D. G. Willis, Trans. Am. Inst. Min. Metall. Eng. **210**, 153 (1957).
[9] J. L. Rubinstein and A. B. Mahani, Seismol. Res. Lett. **86**, 1060 (2015).
[10] S. Roux, J. Schmittbuhl, J. P. Vilotte, and A. Hansen, Europhys. Lett. **23**, 277 (1993).
[11] L. Talon, H. Auradou, and A. Hansen, Phys. Rev. E **82**, 46108 (2010).

[12] L. Talon, H. Auradou, and A. Hansen, Water Resour. Res. **46**, W07601 (2010).

[13] M. Wang, Y.-F. Chen, G.-W. Ma, J.-Q. Zhou, and C.-B. Zhou, Adv. Water Resour. **96**, 373 (2016).

[14] A. Bunde and S. Havlin, eds., *Fractals and Disordered Systems* (Springer Berlin Heidelberg, Berlin, Heidelberg, 1996).

[15] E. Bouchaud, G. Lapasset, and J. Planès, Europhys. Lett. **13**, 73 (1990).

[16] K. J. Måløy, A. Hansen, E. L. Hinrichsen, and S. Roux, Phys. Rev. Lett. **68**, 213 (1992).

[17] J. Schmittbuhl, S. Gentier, and S. Roux, Geophys. Res. Lett. **20**, 639 (1993).

[18] B. L. Cox and J. S. Y. Wang, Fractals-Complex Geom. Patterns Scaling Nat. Soc. **1**, 87 (1993).

[19] J. Schmittbuhl, F. Schmitt, and C. Scholz, J. Geophys. Res. **100**, 5953 (1995).

[20] E. Bouchaud, J. Phys.: Condens. Matter **9**, 4319 (1997).

[21] A. P. Oron and B. Berkowitz, Water Resour. Res. **34**, 2811 (1998).

[22] N. E. Odling, Rock Mech. Rock Eng. **27**, 135 (1994).

[23] D. Amitrano and J. Schmittbuhl, J. Geophys. Res. Solid Earth **107**, 2375 (2002).

[24] L. Ponson, D. Bonamy, and E. Bouchaud, Phys. Rev. Lett. **96**, 35506 (2006).

[25] T. Babadagli, X. Ren, and K. Develi, Int. J. Multiphase Flow **68**, 40 (2015).

[26] M. Sahimi, J. Phys. I France **4**, 1263 (1994).

[27] F. A. L. Dullien, *Porous media: fluid transport and pore structure* (Academic Press, San Diego, 1992).

[28] G. Drazer and J. Koplik, Phys. Rev. E **62**, 8076 (2000).

[29] E. Skjetne, A. Hansen, and J. S. Gudmundsson, J. Fluid Mech. **383**, 1 (1999).

[30] C. C. Mei and J. L. Auriault, J. Fluid Mech. **222**, 647 (1991).

[31] J. C. Wodie and T. Levy, Comptes Rendus L Acad. Des Sci. Ser. Ii **312**, 157 (1991).

[32] P. Forchheimer, Z. Ver. Dtsch. Tsch. Ing. **45**, 1782 (1901).

[33] S. Briggs, B. W. Karney, and B. E. Sleep, J. Rock Mech. Geotech. Eng. **9**, 105 (2017).

[34] E. A. Oliveira, K. J. Schrenk, N. A. M. Araújo, H. J. Herrmann, and J. S. Andrade, Phys. Rev. E **83**, 046113 (2011).

[35] P. A. Morais, E. A. Oliveira, N. A. M. Araújo, H. J. Herrmann, and J. S. Andrade, Phys. Rev. E **84**, 16102 (2011).

[36] B. B. Mandelbrot and J. W. van Ness, SIAM Rev. **10**, 422 (1968).

[37] M. F. Barnsley, R. L. Devaney, B. B. Mandelbrot, H.-O. Peitgen, D. Saupe, and R. F. Voss, *Leonardo*, edited by H.-O. Peitgen and D. Saupe, Vol. 22 (Springer New York, New York, NY, 1988) p. 455.

[38] R. A. Earnshaw, ed., *Fundamental Algorithms for Computer Graphics* (Springer Berlin Heidelberg, 1991).

[39] A. Hansen, J. Schmittbuhl, and G. G. Batrouni, Phys. Rev. E **63**, 62102 (2001).

[40] H. G. Weller, G. Tabor, H. Jasak, and C. Fureby, Comput. Phys. **12**, 620 (1998).

[41] S. Whitaker, Transp. Porous Media **25**, 27 (1996).

[42] M. Sahini, *Appl. Percolation Theory* (CRC Press, Abingdon, UK, 1994).

[43] D. A. Edwards, M. Shapiro, P. Bar-Yoseph, and M. Shapira, Physics of Fluids A: Fluid Dynamics **2**, 45 (1990).

[44] J. S. Andrade, U. M. S. Costa, M. P. Almeida, H. A. Makse, and H. E. Stanley, Phys. Rev. Lett. **82**, 5249 (1999).

[45] R. J. Hill, D. L. Koch, and A. J. C. Ladd, J. Fluid Mech. **448**, 213 (2001).

[46] Y. Chen, W. Liang, H. Lian, J. Yang, and V. P. Nguyen, Int. J. Rock Mech. Min. Sci. **98**, 121 (2017).

[47] T. Ishibashi, N. Watanabe, N. Hirano, A. Okamoto, and N. Tsuchiya, J. Geophys. Res. Solid Earth **120**, 106 (2015).

[48] G. Drazer and J. Koplik, Phys. Rev. E **66**, 26303 (2002).

[49] T. S. Lo and J. Koplik, Phys. Rev. E **89**, 23010 (2014).

[50] N. Huang, Y. Jiang, R. Liu, B. Li, and Z. Zhang, Fractals **25**, 1750051 (2017).